Computational and Theoretical Chemistry 1147 (2019) 29–34

Contents lists available at ScienceDirect

Computational and Theoretical Chemistry

journal homepage: www.elsevier.com/locate/comptc

Molecular dynamics of the interaction of L-tryptophan with polypyrrole oligomers

Maribel Holguín[a], Oscar E. Rojas Álvarez[a,*], Cesar Alberto Arizabaleta[b], Walter Torres[b]

[a] Grupo de Investigación en Química y Biotecnología (QUIBIO) – Universidad Santiago de Cali, Calle 5 # 62-00, Colombia
[b] Grupo de Investigación en Electroquímica – Universidad del Valle, Cali CP760032, Colombia

ARTICLE INFO

Keywords:
Polypyrrole-Trp linkages
Molecular dynamics
Nanomaterials
CHARMM
NAMD
Intermolecular forces

ABSTRACT

There is a current interest in the fabrication of electrochemical sensors based on conducting polymers, such as polypyrrole, (Py)n, for the highly selective sensing of amino acids, for instance, tryptophan, Trp. When (Py)n and other polymers grow in the presence of a target analyte, the material develops cavities that are complementary in size and shape to the analyte. These materials, called molecularly imprinted polymers, MIPs, are very useful for the selective detection of many compounds of biomedical interest. The detailed structure of the MIP complementary cavities is not known. For the design and fabrication of highly selective sensors, information about the structure of such cavities in MIPs is highly desirable. However, this kind of information is not accessible through experimental methods. As a first approach to study the interaction between (Py)n and Trp, in this paper, we use molecular dynamics simulations of Trp and small oligomers of (Py)n (where n = 1, 2, 3, 5) in aqueous solutions. The most significant interactions occur between the indole ring of Trp and the pyrrole pentamer. Attractions occur mainly between the nitrogens of the oligomer chain and the Trp heterocycle, causing the amino acid to walk on the oligomer surface. This process starts with the attraction of Trp by one of the terminal rings in the chain, then, in a concerted way, the nitrogens of the subsequent rings can make a sequence of dipole dipole interactions with the amino acid. Further simulations will address the interaction of Trp with several (Py)n chains simultaneously.

1. Introduction

Tryptophan (Trp, Fig. 1a) is an essential amino acid, precursor of a series of molecules with neurological activity, namely serotonin, a mood regulator; melatonin, which participates in signaling sleep cycles; kynurenic acid (KINA), which prevents degeneration of nerve cells; and 3-hydroxykynurenine (3-HK), a neurotoxic. Some studies show that the relative concentrations of KINA and 3-HK in the brain may play an important role in Parkinsońs and Alzheimeŕs diseases [1].

Given Trp biochemical and nutritional importance, analytical methods have been developed for the determination of this amino acid [2]. A typical problem is that Trp readily degrades during the analysis routines, which leads to inaccuracies in the results. Thus, the development of non destructive, low cost analytical methods that can be used in biological fluids is highly desirable.

Molecularly imprinted polymers (MIPs) are materials of interest for the fabrication of highly selective sensors towards a wide variety of analytes. MIPs are polymers that grow in a medium that also contain some target molecules and crosslinking agents in porogenic solvents. The polymer grows around these target molecules and so they behave as templates. Removal of the template after polymerization creates cavities in the polymer network that are complementary in size and shape to the templates. The crosslinker influences the morphology and mechanical stability, thus helping to preserve the cavities in the polymer, which can then recognize the templates with high selectivity. Because of their molecular recognition capabilities, MIPs are also called plastic antibodies.

MIPs have been synthesized mainly by conventional free-radical polymerization or copolymerization synthetic routes and, more recently, by controlled radical polymerization methods. Many acrylate derivatives and others have been used as crosslinkers [3]. MIPs can also be prepared by electrochemical synthesis of conducting polymers such as polypyrrole, polyaniline, and others [4]. Conducting polymer films deposited on electrodes can reversibly switch from an insulating to a conducting state by control of the electrode potential. The redox state change is accompanied by ion exchange (cations or anions) with the contacting medium and changes in the hydrophilicity/hydrophobicity of the polymer surface.

* Corresponding author.
E-mail address: oerojas@usc.edu.co (O.E. Rojas Álvarez).

https://doi.org/10.1016/j.comptc.2018.11.012
Received 25 September 2018; Received in revised form 20 November 2018; Accepted 29 November 2018
Available online 30 November 2018
2210-271X/

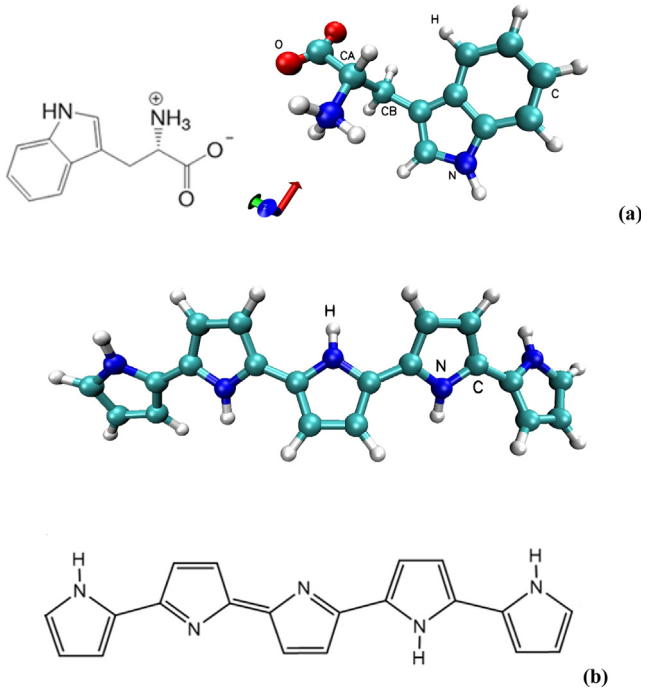

Fig. 1. Chemical structure of (a) the zwitterion form of L-tryptophan (Trp), (b) Polypyrrole $(Py)_5$. The zwitterion form of L-Trp is the predominant species in aqueous solutions in the pH range between 4 and 8, approximately.

Polyprrole (Py)n, (Fig. 1b) has been widely used in the preparation of MIPs for the detection of many analytes of biomedical interest, including caffeine, adenosine, and amino acids such as aspartic acid (Asp) and Trp.

The structure of reduced and oxidized polypyrrole has been characterized through experimental, quantum mechanics and molecular dynamics methods. These studies reveal aspects of ion and solvent transport [5–7] through thin films and relaxation of the polymer chains [8].

Recently, molecular dynamics methods have been used to obtain information on the interaction between MIPs and template molecules at the molecular level [9]. This kind of information is not accessible through experimental methods and it is useful for the rational design of MIPs [10].

We are interested in MIP-based electrochemical sensors for Trp and Trp metabolites. Information on the molecular level interactions of Trp with polypyrrole chains will help us to understand the structure of the complementary cavities, which, in turn, may help to improve the sensitivity, selectivity, and long term stability of these MIPs.

In this work, we discuss the molecular dynamics simulation of neutral pyrrole and small oligomers, (Py)n, where n = 2, 3 and 5, in aqueous solutions that also contain L-Trp. The simulation shows significant interactions between the indole ring of L-Trp and the pyrrole pentamer.

2. Computational methods

In this work, the solvent molecules are implicit. Thus, water molecules are not included in the simulation and an effective, distance dependent, dielectric constant is used, $\varepsilon_{eff} = r_{ij}$. A TIP3 implicit water simulation with a 10 Å rigid cubic cell measured from the atom with the largest coordinate in every direction. Table 1 shows the number of water molecules used in all simulations.

The structures (PDB files) and coordinates (PSF files) were generated from topologies and initial force field parameters obtained from the Protein Data Bank (RCSB) [11] for L-Trp used in all simulations and the pyrrole monomer used in simulation A. For the (Py)n oligomers in simulations B, C, and D, the structures, topologies, and force field parameters were obtained from the Swiss Institute of Bioinformatics [12] The initial orientation was attained with Swiss.pdb Viewer. CHARMM force fields were used all throughout [13–16].

Table 1
Description of the carried simulations.

Simulation	(Py)n (n = number of rings)	Number of water molecules	Simulation time (ps)
A	1	489	3000
B	2	546	
C	3	558	
D	5	790	

To include long range electrostatic interactions in the simulations, the particle mesh Ewald method for periodic systems was used. It creates a 3D grid over which the charge is distributed. Grid size was configured to 1 Å.

The values corresponding to the periodic boundary conditions were set to those of the water box [13,17].

The energy of the Trp(Py)n complex was minimized every 100 steps with a 12 Å cutoff. The MD simulation visualization file was set to 250 steps per visualization.

The simulation time was 3000 ps with 1 fs per step (3000000 steps). The temperature and pressure were 310 K and 1 atm, respectively, for an isobaric-isothermal ensemble.

In this work, the Visual Molecular Dynamics (VMD 1.9.3) for visualization and the Scalable Molecular Dynamics (NAMD 2.12) simulation software were used.

The phase point equilibrium runs the simulation until properties get stable with respect to time. Average energy routine parameters were calculated as stated in Eq. (1):

$$E = \frac{1}{N}\sum_{i=1}^{N} Ei \tag{1}$$

and RMSD in Eq. (2):

$$RMSD = \sqrt{\sum_{i=1}^{N\ \ atoms} \frac{(ri(t1) - ri(t2))^2}{N\ \ atoms}} \tag{2}$$

where *N atoms* is the numbers of atoms whose positions are being compared, and *ri(t)* is the position of atom *i* at time *t*.

3. Results and discussion

3.1. Optimized structures for polypyrrole and Trp

Five optimized structures were obtained at the Protein data bank (RCSB), namely, L-Trp, molecular pyrrole and three small (Py)n oligomers. These structures were compared to geometric parameters of computational and theoretical studies [8,18–20]. The increase in ring number did not considerably affect bond lengths and angles or the dihedral angles [18].

Four simulations were performed for the complexes between L-Trp and the oligomers as shown in Table 1.

The final simulated structures were oriented with respect to the mass center of (Py)n and L-Trp in order to optimize the number of intermolecular attractions, then energy minimization was performed by fixing L-Trp in several positions around the oligomer chain. Finally, the correct position of L-Trp with optimized energies for every simulation was obtained (Fig. 2(a)–(d)). After energy optimization of the oligomers, the pyrrole rings exhibit an alternate conformation (*anti-gauche*), with the nitrogen atoms in neighboring rings pointing at opposite directions.

This is the most stable conformation for pyrrole rings according to experimental results and calculations at different levels of theory [21].

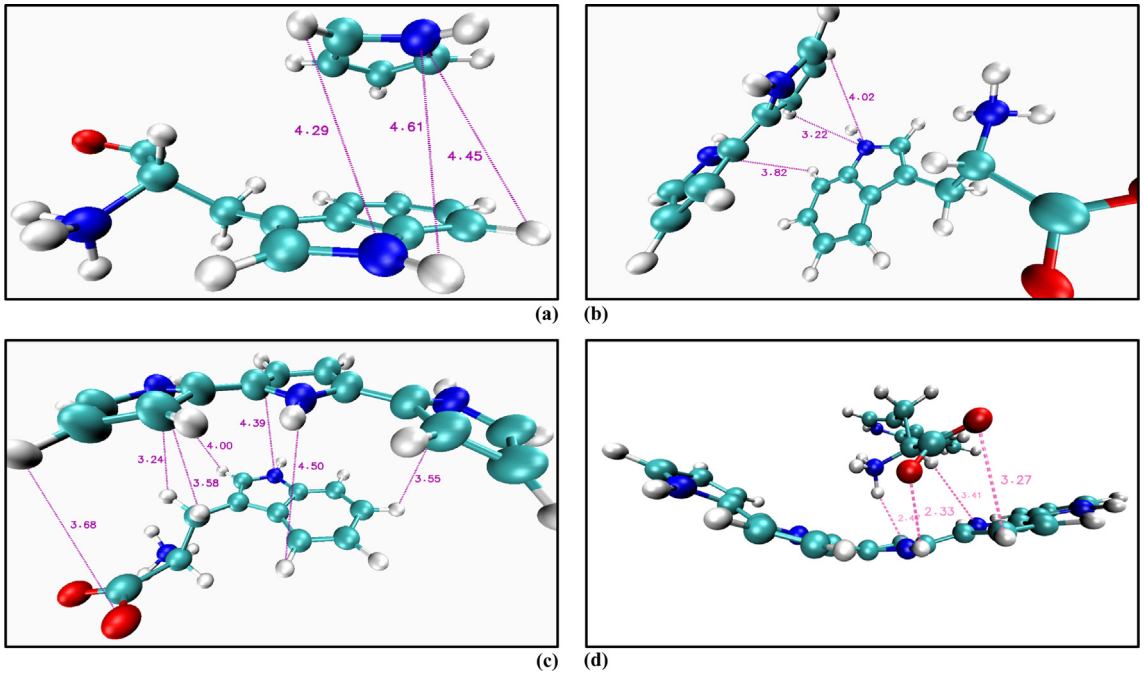

Fig. 2. Initial positions oriented with respect to the mass center, after energy minimization and average distances between (Py)n and L-Trp for (a) A 4,4 Å. (b) B 3,6 Å. (c) C 3,7 Å. (d) D 2,9 Å.

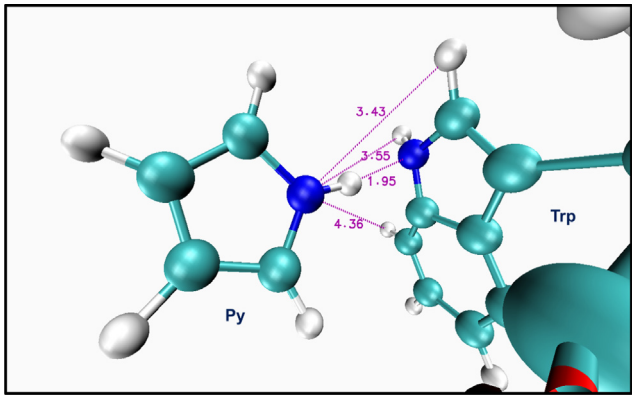

Fig. 3. Attractive atomic interactions between L-Trp and Py. Trp: HD1-Py:N5 3,43 Å; Trp:HE1-Py:N5 3,55 Å; Trp:NE1-Py:H5 1,95 Å; Trp:HZ2-Py:N5 4,36 Å.

As shown in Figs. 1 and 2, the zwitterion form of Trp is used throughout the simulation because it is the most stable species in aqueous solutions in the pH range from 4 to 8, approximately.

3.2. RMSD simulations

During the first few picoseconds of all simulations, the root mean square deviation (RMSD) analysis shows a dipole-dipole electrostatic interaction that depends on the initial orientation. But this interaction is lost as the simulation proceeds. Simulations A, B and C show very short, although frequent attractions. In simulation D, however, the intermolecular attractions last longer but are less frequent than those in A, B, and C. The atomic fluctuations and weak forces between Trp and (Py)n increase with the number of rings, which results from the higher degrees of freedom at the non- binding zone. At the molecular level, the analysis of these weak forces can be performed by using quantum chemistry approaches such as bond critical points or energy decomposition analysis combined with the natural orbitals for chemical valence theory [25].

In simulation A, (RMSD, Fig. 5) an atomic fluctuation is observed in

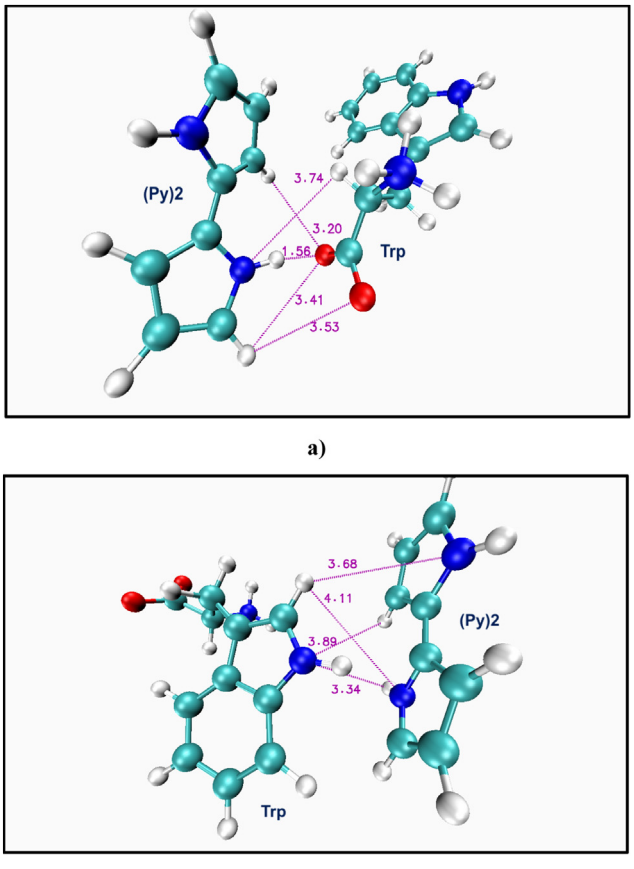

Fig. 4. Interactions in simulation B (a) Five attraction points $(Py)_2$:H-Trp:OT1 3,53 Å; (Py)2:H-Trp:OT2 3,41 Å; (Py)2:H6-Trp:OT2 1,56 Å; (Py)2:N-Trp:HA 3,74 Å; Trp:OT2-(Py)2:H3 3,20 Å. (b) Four-attraction points Trp:NE1-(Py)2:H7 3,29 Å; Trp:NE1-(Py)2:H1; (Py)2:N1-Trp:HD1 3,30 Å; Trp:HD1-(Py)2:N 4,09 Å.

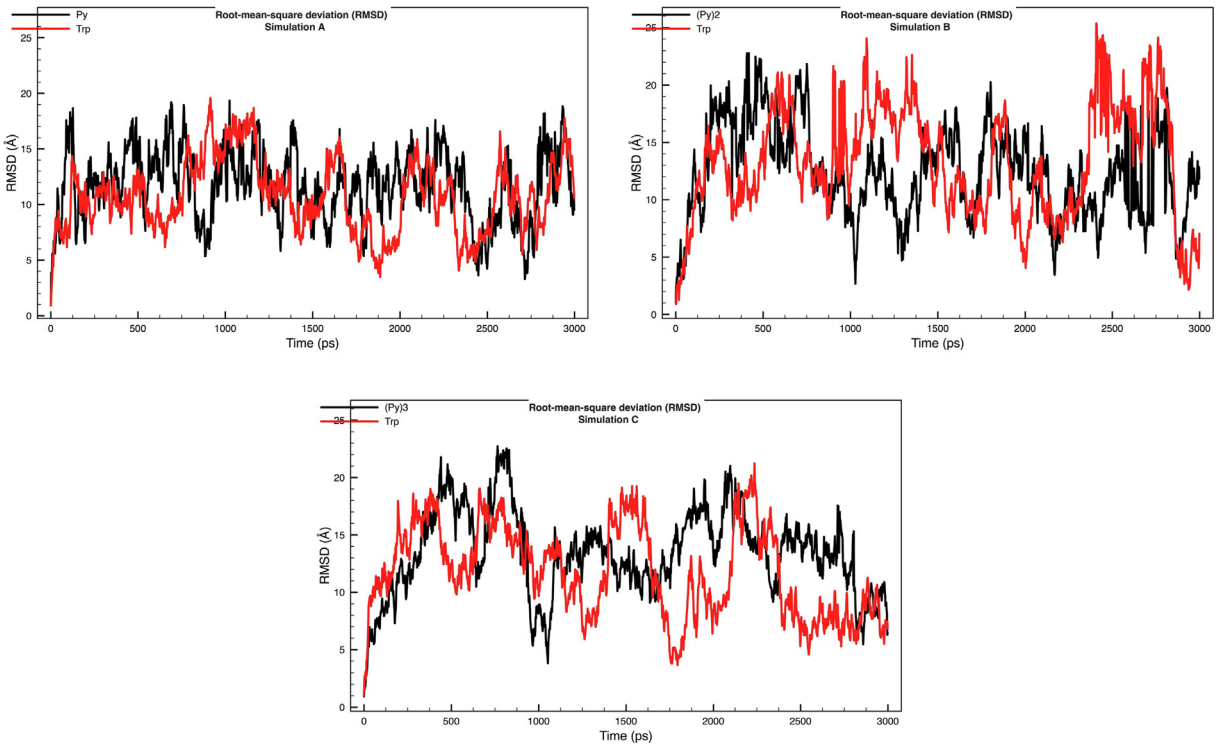

Fig. 5. RMSDs for simulations A, B, and C. Trp in red and (Py)n in black (n = 1,2,3). (For interpretation of the references to colur in this figure legend, the reader is referred to the web version of this article.)

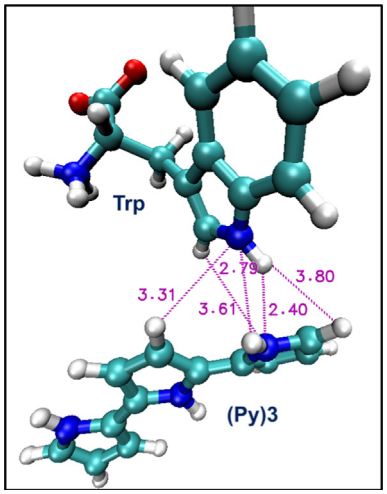

Fig. 6. Simulation C. Five point atomic attractions. Trp:HZ2-$(Py)_3$:N2 2,87 Å; $(Py)_3$:N2-Trp:HE1 3,09 Å; $(Py)_3$:H10-Trp:NE1 3,70 Å; Trp:NE1-$(Py)_3$:H4 3,73 Å; Trp:HE1-$(Py)_3$:N1 3,07 Å.

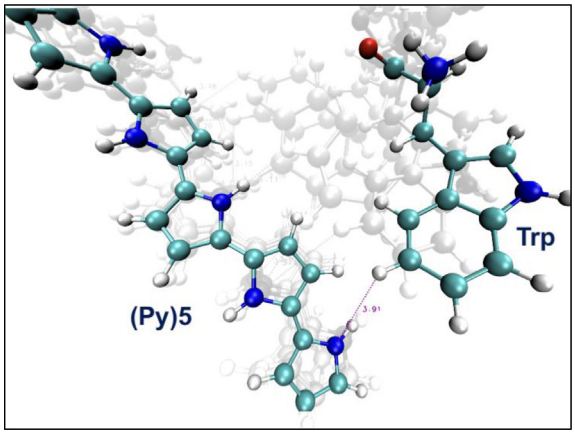

Fig. 7. Attractions in simulation E. Sequential displacement of Trp (a1) Trp:HZ3-(Py)5:N4 3,91 Å. (a2) Trp:HH2-(Py)5:N2 3,74 Å; Trp:HZ3-(Py)5:N1 4,11 Å. (a3) Trp:NE1-(Py)5:H5 3,82 Å; Trp:HZ2-(Py)5:N1 3,33 Å; (Py)5:N1-Trp:HH2 3,03 Å; Trp:HH2-(Py)5:N 4,04 Å (b) Five contact points Trp:OT1-(Py)5:H16 3,25 Å; Trp:OT2-(Py)5:H13 3,38 Å: Trp:OT2-(Py)5:H16 1,58 Å; Trp:OT2-(Py)5:H 2,61 Å; (Py)5:H4-Trp:NE1 3,36 Å.

the range between 5 and 20 Å, which is stable throughout the simulation, specially for Trp. Other variable moments of attraction were observed but were discarded because they did not exceed 7 ps. In contrast, two intervals, between (2412–2430) ps and (2457–2489) ps, in which the molecular attractions were stable and constant, can be highlighted (see Fig. 3).

In simulation A (Fig. 3), the strongest interaction is between Py:H5 and Trp:NE1 due to the electronegativity of the N atoms. Observe that there is a slight torsion between the two rings in L-Trp and that the peptide region points away from the Py ring. During the interaction, the Trp rings are perpendicular to the NH bond in Py. Overall, the main intermolecular interactions correspond to hydrogen bonds between the endocyclic nitrogen of L-Trp and all of the hydrogen atoms of Py (Trp:NE1 - Py:H1, H2, H3, H4 and H5) and between the Py nitrogen (Py:N5) and some of the hydrogens in the Trp indole ring Trp:HE1, HD1 and HZ2. However, these interactions rapidly lose strength, meaning that the N——H—C is not sufficiently strong to hold the Py ring in one position because the C—H groups and the Py resonant system act as weak hydrogen donors and acceptors, respectively.

In simulation B, the RMSD (Fig. 5) is relatively stable, slightly fluctuating around 10 Å. The longest attraction interval last 89.5 ps (796–881 ps), followed by a 66.2 ps interval (2858–2924 ps) as seen in Fig. 4. In the interval from 796 to 881 ps, the N———H—O and N——H—N interactions are noticeable, making $(Py)_2$ to move from the indole ring to the peptidic side of Trp; this behavior is the same for the two Py rings without loss of atomic attraction.

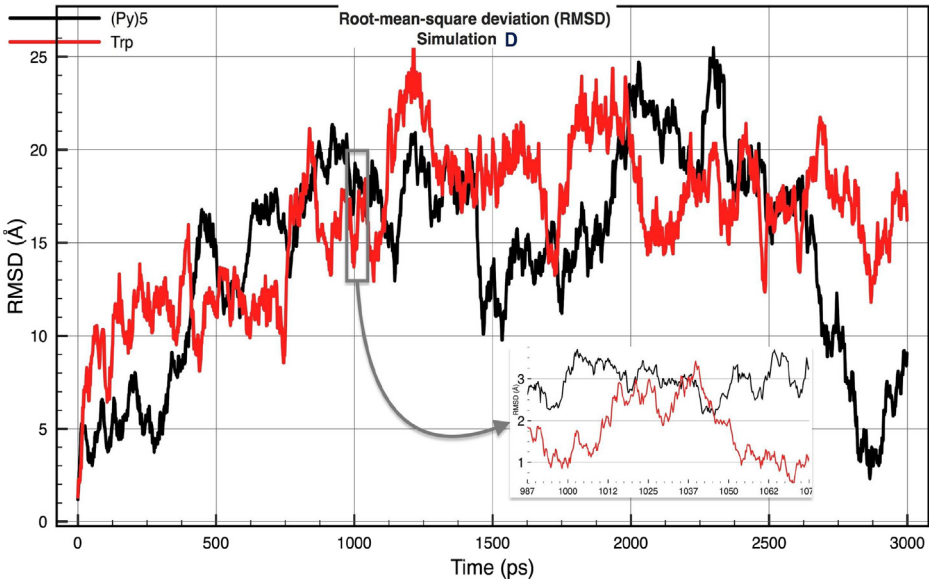

Fig. 8. RMSD for simulation D. (Py)5 and Trp in black and red lines, respectively. The inset shows the interval 992–1063 ps where the waking effect is observed. (For interpretation of the references to colur in this figure legend, the reader is referred to the web version of this article.)

The main intermolecular attractions involved the two oxygen atoms of Trp: O2 Trp: O1 and $(Py)_2$: H6, H3 and H or Py: H7, H2 and H5 making contact with at least three atoms, Trp: NE1 and $(Py)_2$: H6, H3 or Py: H7, H2. Interactions were also observed between $(Py)_2$: N, N1 and some of the hydrogens of the Trp heterocycle with at least two contact points (Fig. 4).

Notice that, in simulation B, Trp showed four electrostatic interactions, that involve N and H atoms, with several atoms of $(Py)_2$, whereas, in simulation A, Trp presented multiple electrostatic attractions, *via* H and O atoms, with the N and the H atoms in Py. The Trp-Py attraction is rapidly lost because the occupation of the single electronegative atom of Py allows the movement of the rest of the Py molecule that is not retained by any other Trp site.

In simulation C, the RMSD shows molecular fluctuations at around 13 Å. Relevant molecular interactions happen in the time intervals (1367–1400) ps and (1125–1175) ps (Fig. 5). The most noteworthy molecular interactions are those among the nitrogen atoms in $(Py)_3$ and the H atoms in the Trp heterocycle, evidencing, once again, that the N−H———N hydrogen bonds are stronger than the N——H−C ones (Fig. 6).

In simulation D, in the interval (992–1063) ps, the interaction is such that Trp moves over the $(Py)_5$ chain, where the N atoms of the oligomer: N, N1, N2, and N4 interact in a coordinated manner with Trp: HZ3, HH2, and HZ2. The interaction sites involve two to five electrostatic attractions (Fig. 8).

The main intermolecular attractive interactions are those between H and N atoms, and, to a lesser degree, between O and H atoms. Taking into account van der Waals forces, the maximum distance for attraction was set to 4 Å. Comparing simulations A and D, while in the former, the position of Trp rings is parallel to the cartesian plane of Py, in the later, the position of Trp allows the Trp ring to stand close to the $(Py)_5$.

One of the most important characteristics of the molecular dynamics of simulation D is that attractions occur mainly between the nitrogens of the oligomer chain and the Trp heterocycle, that generates a "walking" effect for the amino acid on the oligomer surface (Fig. 7). This process starts with the attraction of Trp by one of the terminal rings in the chain, then, in a concerted way, the nitrogens of the subsequent rings can make a sequence of dipole dipole interactions with the amino acid. The attraction is generated along four consecutive Py rings and then Trp returns to the starting point. Interestingly, Density Functional Theory (DFT) calculations in surfaces consider that the interactions N−H—N are not stable because of stacking [24], but Trp's ability to gain and lose affinity at several points of the oligomer at the same time, provides it with some stability.

Finally, as the number of rings increases in the oligomer chain, the fluctuations become more stable, rotation of the dihedral angle located at the beta carbon (CB) in Trp, allows the Trp ring to stand close to the (Py)n surface, producing an increased number of interaction points between Trp and (Py)n.

A theoretical study based on molecular dynamics made use of this polymer as an ammonium gas sensor [18] and determined that the presence of the analyte not only manages to generate intermolecular interactions of hydrogen bonds N−H with polypyrrole, but also induces a change in the dihedral angles. Furthermore, several simulations have shown the ability of L-tryptophan to interact through hydrogen bonds in protein-lipid complexes [22,23].

4. Conclusions

Strong interactions between L-Trp and the (Py)n oligomers occur mainly through the N−H bonds in the oligomers and the N−H bonds in Trp. The interactions last for several tens of ps but the time of the interactions and the number of dipole dipole attractions and hydrogen bonds increase with the oligomer chain size.

$(Py)_5$ induces the L-Trp molecule to walk over the pyrrole rings because of intermolecular interactions N——H−N y N——H−C between the Py rings and the indole group. Rotation of the dihedral angle located at the beta carbon (CB) in Trp allows the indole bicyclic ring of Trp to stand close to the (Py)n surface, which, in turn, increases the number of interaction points between Trp and (Py)n.

The current study does not suggest that one single (Py)n chain espontaneously wraps around the L-Trp molecule. Thus, in order to understand the formation of complementary cavities of L-Trp and polypyrrole, further work will address the simultaneous interaction of the amino acid with several (Py)n chains.

Acknowledgments

This research project was supported by Universidad del Valle, Universidad Santiago de Cali and the Departamento Administrativo de Ciencia, Tecnología e Innovación (COLCIENCIAS) (grant number 647-2014).

Appendix A. Supplementary data

Supplementary data to this article can be found online at https://doi.org/10.1016/j.comptc.2018.11.012.

References

[1] C. Breda, K.V. Sathyasaikumar, S. Sograte Idrissi, F.M. Notarangelo, J.G. Estranero, G.G.L. Moore, E.W. Green, C.P. Kyriacou, R. Schwarcz, F. Giorgini, Tryptophan-2,3-dioxygenase (TDO) inhibition ameliorates neurodegeneration by modulation of kynurenine pathway metabolites, Proc. Natl. Acad. Sci. 113 (2016) 5435–5440, https://doi.org/10.1073/pnas.1604453113.

[2] I. Sadok, A. Gamian, M.M. Staniszewska, Chromatographic analysis of tryptophan metabolites, J. Sep. Sci. 40 (2017) 3020–3045, https://doi.org/10.1002/jssc.201700184.

[3] P.A.G. Cormack, A.Z. Elorza, Molecularly imprinted polymers: synthesis and characterisation, J. Chromatogr. B Anal. Technol. Biomed. Life Sci. 804 (2004) 173–182, https://doi.org/10.1016/j.jchromb.2004.02.013.

[4] P.S. Sharma, A. Pietrzyk-le, Electrochemically synthesized polymers in molecular imprinting for chemical sensing, Anal. Bioanal. Chem. 402 (2012) 3177–3204, https://doi.org/10.1007/s00216-011-5696-6.

[5] J.J. López Cascales, A.J. Fernández, T.F. Otero, Characterization of the reduced and oxidized polypyrrole/water interface: a molecular dynamics simulation study, J. Phys. Chem. B 107 (2003) 9339–9343, https://doi.org/10.1021/jp027717o.

[6] J.J. López Cascales, T.F. Otero, Molecular dynamics simulations of the orientation and reorientational dynamics of water and polypyrrole rings as a function of the oxidation state of the polymer, Macromol. Theory Simulat. 14 (2005) 40–48, https://doi.org/10.1002/mats.200400066.

[7] S.D. Oliveira Costa, J.J. López Cascales, Molecular dynamics simulation of polypyrrole film in an acetonitrile solution, J. Electroanal. Chem. 644 (2010) 13–19, https://doi.org/10.1016/j.jelechem.2010.03.022.

[8] J.M. Fonner, C.E. Schmidt, P. Ren, A combined molecular dynamics and experimental study of doped polypyrrole, Polymer (Guildf) 51 (2010) 4985–4993, https://doi.org/10.1016/j.polymer.2010.08.024.

[9] Y. Kong, N. Wang, X. Ni, Q. Yu, H. Liu, W. Huang, W. Xu, Molecular dynamics simulations of molecularly imprinted polymer approaches to the preparation of selective materials to remove norfloxacin, J. Appl. Polym. Sci. 133 (2016) 1–11, https://doi.org/10.1002/app.42817.

[10] T. Cowen, K. Karim, S. Piletsky, Computational approaches in the design of synthetic receptors – a review, Anal. Chim. Acta 936 (2016) 62–74, https://doi.org/10.1016/j.aca.2016.07.027.

[11] H.M. Berman, J. Westbrook, Z. Feng, G. Gilliland, T.N. Bhat, H. Weissig, I.N. Shindyalov, P.E. Bourne, The protein data bank, Nucleic Acids Res. 28 (2000) 235–242, https://doi.org/10.1093/nar/28.1.235.

[12] V. Zoete, M.A. Cuendet, A. Grosdidier, O. Michielin, SwissParam: a fast force field generation tool for small organic molecules, J. Comput. Chem. 32 (2011) 2359–2368, https://doi.org/10.1002/jcc.21816.

[13] J.C. Phillips, R. Braun, W. Wang, J. Gumbart, E. Tajkhorshid, E. Villa, C. Chipot, R.D. Skeel, L. Kalé, K. Schulten, Scalable molecular dynamics with NAMD, J. Comput. Chem. 26 (2005) 1781–1802, https://doi.org/10.1002/jcc.20289.

[14] A.D. Mackerell, M. Feig, C.L. Brooks, Extending the treatment of backbone energetics in protein force fields: limitations of gas-phase quantum mechanics in reproducing protein conformational distributions in molecular dynamics simulation, J. Comput. Chem. 25 (2004) 1400–1415, https://doi.org/10.1002/jcc.20065.

[15] A.D. MacKerell, D. Bashford, M. Bellott, R.L. Dunbrack, J.D. Evanseck, M.J. Field, S. Fischer, J. Gao, H. Guo, S. Ha, D. Joseph-McCarthy, L. Kuchnir, K. Kuczera, F.T.K. Lau, C. Mattos, S. Michnick, T. Ngo, D.T. Nguyen, B. Prodhom, W.E. Reiher, B. Roux, M. Schlenkrich, J.C. Smith, R. Stote, J. Straub, M. Watanabe, J. Wiórkiewicz-Kuczera, D. Yin, M. Karplus, All-atom empirical potential for molecular modeling and dynamics studies of proteins †, J. Phys. Chem. B. 102 (1998) 3586–3616, https://doi.org/10.1021/jp973084f.

[16] W. Yu, X. He, K. Vanommeslaeghe, A.D. MacKerell, Extension of the CHARMM general force field to sulfonyl-containing compounds and its utility in biomolecular simulations, J. Comput. Chem. 33 (2012) 2451–2468, https://doi.org/10.1002/jcc.23067.

[17] W.L. Jorgensen, J. Chandrasekhar, J.D. Madura, R.W. Impey, M.L. Klein, Comparison of simple potential functions for simulating liquid water, J. Chem. Phys. 79 (1983) 926–935, https://doi.org/10.1063/1.445869.

[18] H. Ullah, K. Ayub, Z. Ullah, M. Hanif, R. Nawaz, A.U.H.A. Shah, S. Bilal, Theoretical insight of polypyrrole ammonia gas sensor, Synth. Met. 172 (2013) 14–20, https://doi.org/10.1016/j.synthmet.2013.03.021.

[19] J.M. Ribo, C. Acero, M.C. Anglada, A. Dicko, On the structure and transport properties of polypyrroles, Bull. Soc. Cat. Cien. 13 (1992).

[20] I. Rabias, B.J. Howlin, Combined ab initio and semi-empirical study on the theoretical vibrational spectra and physical properties of polypyrrole, Comput. Theor. Polym. Sci. 11 (2001) 241–249, https://doi.org/10.1016/S1089-3156(00)00010-6.

[21] S. Millefiori, A. Alparone, Theoretical study of the structure and torsional potential of pyrrole oligomers, J. Chem. Soc. - Faraday Trans. 94 (1998) 25–32, https://doi.org/10.1039/a705780f.

[22] J. Marti, H. Lu, Molecular dynamics of di-palmitoyl-phosphatidyl-choline biomembranes in ionic solution: adsorption of the precursor neurotransmitter tryptophan, Proc. Comput. Sci. 108 (2017) 1242–1250, https://doi.org/10.1016/j.procs.2017.05.141.

[23] K.M. Sanchez, G. Kang, B. Wu, J.E. Kim, Tryptophan-lipid interactions in membrane protein folding probed by ultraviolet resonance Raman and fluorescence spectroscopy, Biophys. J. 100 (2011) 2121–2130, https://doi.org/10.1016/j.bpj.2011.03.018.

[24] Titas Kumar Mukhopadhyay, Kalishankar Bhattacharyya, Ayan Datta, Gauging the nanotoxicity of h2D–C2N toward single-stranded DNA: an in Silico molecular simulation approach, ACS Appl. Mater. Interf. 10 (16) (2018) 13805–13818.

[25] Sk Jahiruddin, Nilangshu Mandal, Ayan Datta, Structure and electronic properties of unnatural base Pairs: the role of dispersion interactions, ChemPhysChem 19 (2018) 67–74.